Physica D 454 (2023) 133839

Contents lists available at ScienceDirect

Physica D

journal homepage: www.elsevier.com/locate/physd

Astrocytic clearance and fragmentation of toxic proteins in Alzheimer's disease on large-scale brain networks

Hina Shaheen [a,*], Swadesh Pal [a], Roderick Melnik [a,b]

[a] MS2 Discovery Interdisciplinary Research Institute, Wilfrid Laurier University, Waterloo, Canada
[b] BCAM - Basque Center for Applied Mathematics, E-48009, Bilbao, Spain

ARTICLE INFO

Article history:
Received 16 November 2022
Received in revised form 28 March 2023
Accepted 8 May 2023
Available online 13 July 2023
Communicated by T. Lorenzi

Keywords:
Large-scale brain networks
Alzheimer's disease
Nonlinear Smoluchowski equation
Multiscale modelling

ABSTRACT

The human brain is the most complicated biological structure on the planet. A major challenge of brain network modelling lies in its multi-scale spatio-temporal nature, covering scales from synapses to the whole brain. The coupled multiphysics and biochemical activities which spread through such a complex system shape brain capacity inside a structure-function relationship that requires a particular mathematical framework. Next-generation coupled-based mathematical modelling approaches to brain networks and the analysis of data-driven dynamical systems are needed to advance state-of-the-art therapeutic strategies for treating neurodegenerative diseases (NDDs) that affect millions of people worldwide, such as Alzheimer's disease (AD) and Parkinson's disease (PD). Importantly, AD is marked by the presence of amyloid-beta ($A\beta$) plaques and tau (τ) proteins. Some disease-specific misfolded proteins can interact with healthy proteins to form long chains and aggregates of different sizes that have different transport properties and toxicity. An improved large-scale brain network model is proposed here to understand the pathogenesis of AD, especially the role of astrocytes in the presence of misfolded proteins ($A\beta$ and τ). The idea involves astrocytic clearance, which assists in eliminating toxic $A\beta$ via fragmentation. We use the general Smoluchowski theory of nucleation, aggregation, and fragmentation to predict the development and propagation of aggregates of misfolded proteins in the brain. It has been shown that the developed model leads to different size distributions and propagation along the network. We predicted that astrocytic clearance varies with the aggregate size, which is key to slowing down AD progression. The clearance and fragmentation of toxic proteins span several spatial and temporal scales, and this research will potentially yield new insight into the associated processes and brain networks in health and disease. Detailed multi-scale brain modelling provides a promising approach for consolidating, organizing, and bridging the data sets of data-driven brain network models.

1. Introduction

The network architecture of the human brain has attracted the attention of the neuroscientific community due to its ability to shed light on human cognition, its variation during development and ageing, and its modification in disease or injury [1]. A human brain comprises around 100 billion neurons coupled by approximately 100 trillion synapses that are physically structured across various spatial dimensions and functionally interacting over many temporal scales [2]. Researchers have found that discrete populations of neurons support cognition and behaviour, and individual brain areas have progressively given rise to the understanding that connectivity matters [3–6]. The realization that large-scale brain networks are inherently multi-scale structures is one of the most recent advances [1]. To determine which combinations of interacting regions are possible, it is necessary to identify the brain areas that compose structural network nodes and the connecting pathways that function as structural network edges.

In recent years, mathematical and computational methods have paved the way towards a much better understanding of brain functional connectivity [7,8]. It is known that neurodegenerative diseases (NDDs) involve large networks, and we need to reduce such large networks to make them feasible for a more detailed analysis. Functional interactions in the brain are constrained by the underlying anatomical architecture, and structural and functional networks share network features such as modularity [9,10]. Furthermore, understanding brain geometry by mapping its functional and structural associations has been rapidly developing, generating enormous interest [11]. Interestingly, neuroscientists employ network science methods to represent the brain as a network and a mathematical representation of data ideally suited for investigating complex systems [12,13]. Connectomics and graph theory provide an effective paradigm for

* Corresponding author.
E-mail addresses: shah8322@mylaurier.ca (H. Shaheen), spal@wlu.ca (S. Pal), rmelnik@wlu.ca (R. Melnik).

https://doi.org/10.1016/j.physd.2023.133839
0167-2789/

mapping, monitoring, and predicting disease spread patterns in brain diseases [14,15]. The therapeutic importance of brain network hubs is one major insight that has already been made with the remarkable consistency of MRI connectomics [16,17]. It has been demonstrated that in Alzheimer's disease (AD), high-degree nodes in functional MRI graphs have more local deposition of amyloid protein (measured via PET) than less topologically central brain areas [18]. Importantly, NDDs represent a heterogeneous group of diseases characterized by progressive structural and functional degeneration of the central and peripheral nervous systems [19]. Throughout growth, the healthy human brain builds a series of large-scale, dispersed, function-critical neural networks. NDDs are thought to focus on these networks, but this hypothesis has not been systematically tested in living humans [20]. Biomarkers in NDDs and their integration into modelling procedures have risen as an important tool for shedding light on the pathophysiology of NDDs. The pathophysiology of NDDs is still debated, and there is an urgent need to understand the mechanisms behind the onset and progression of these heterogeneous diseases, where AD and Parkinson's disease (PD) are noteworthy causes of morbidity and mortality around the world [21,22]. AD is one of the foremost chronic diseases of the central nervous system (CNS), characterized by memory loss and cognitive dysfunction. It exhibits certain neurological and psychiatric symptoms and behavioural disorders [23]. Protein aggregates are found in postmortem brain tissues afflicted by NDDs [24]. Pathologically, AD is marked by the presence of extracellular amyloid plaques ($A\beta$), and intracellular neurofibrillary tangles (NFTs) of tau protein (τ) within the brain [25]. The reason behind AD is assumed to be impairment of the link between neuronal and astrocytic (non-neuronal) functions in brain regions related to memory or thinking (such as the hippocampus) [26].

Astrocytes, or astroglia, are another kind of glial cells that play a role in synapse development and ion homeostasis. They are also connected to the brain immune system [21]. Astroglia operates as an immune cell type in a healthy brain, but when AD is present, they can act differently. Astroglia becomes activated and reactive in the presence of AD [27]. Importantly, astrocyte reactivity is a defining feature of neuroinflammation, which occurs in AD and practically every other NDDs [28]. This reactivity of astrocytes also promotes degeneration and intracellular protein aggregation [29]. NDDs tend to progress in a predictable pattern through the brain, for instance, in AD τ aggregates are first discovered in the locus coeruleus and entorhinal cortex, then spreading to the hippocampus, temporal cortex, and parietal cortex before entering the motor cortex and occipital brain regions [24]. The protein aggregates are the foundation of the prion-like hypothesis for NDDs [30]. This process is based on the assumption that like prion diseases [24,25], NDDs are produced by the systematic aggregation and transport of misfolded proteins in the brain via axonal pathways [24,31,32]. It is specifically applicable to protein aggregates observed in AD. Species like monomeric, oligomeric, and fibrillar activate astrocytes, which can result in neuronal death [33]. τ proteins are normally generated by the cell in healthy tissue, but in some circumstances, these proteins begin to form misfolded aggregates, and this misfolded version of the protein works as a toxic template on which regular proteins can be bound and transformed to misfolded ones. Since τ is an intracellular protein, these various huge aggregates travel largely across the brain via a network of axonal channels [34–36], and numerous methods of cell–cell spreading have been found ([24] and references therein). $A\beta$, on the other hand, is known to form large extracellular aggregates [37–39]. We know from diffusion tensor imaging that diffusion is preferentially along the axons if these aggregates are carried inside the brain as a simple diffusion process. Importantly, in most models of AD, the focus is on the development of $A\beta$ fibrils, which are assumed to be the primary pathogenic factor for cell death. Murphy and Pallitto, for example, proposed a homogeneous Smoluchowski model that was validated using kinetic experiments [40]. Additionally, Bertsch et al. [41] considered and implemented a model for the accumulation and distribution of $A\beta$ in a brain slice geometry. Matthäus also discretized and analysed similar equations on networks [42]. Therefore, building on these earlier works, we develop a broad framework to study toxic protein propagation in the brain represented as a network based on the prion-like hypothesis of NDDs. Since $A\beta$ and τ proteins are considered as a hallmark of AD [21], we will illustrate the NDD's model based on both $A\beta$ and τ proteins on a large-scale brain network. The network model is constructed from a coarse-grained continuum model. Note that the fragmentation comes from astrocytes, where astrocytes play an important role in clearing $A\beta$ [27]. However, in the present study, we assume that astrocytes do not clear the toxic τ proteins. The simplifying assumptions we make for the present study are adopted from [24] while maintaining crucial properties of known mechanisms.

As a result, we investigate the propagation of intracellular protein aggregates across the brain using Smoluchowski's aggregation theory [24]. Our special attention is given to how coarse-grained models might be utilized to capture the complicated underlying dynamics of astrocytes' role in AD. The continuous equations are initially formulated using anisotropic diffusion, and then the equations are discretized on a large-scale brain network.

2. General theory and mathematical modelling approach

In this section, we first discuss the theory behind the general Smoluchowski model for aggregation and fragmentation of toxic proteins, and then we develop the general and continuous Smoluchowski model for NDDs.

2.1. Smoluchowski's model for NDDs

The mathematical models are important in order to study the kinetics of misfolding proteins, for instance, the simple one-concentration Fisher–Kolmogorov model [43], the two-concentration heterodimer model [44] and the n-concentration Smoluchowski model [25,45]. Before getting into the problem of proteins in the brain, it is worth briefly recasting Smoluchowski's general theory of particle aggregation and fragmentation in space and time [45]. Firstly, we will consider the continuum case and then discretize these equations on a large-scale brain network. Let C_i be the aggregates and c_i be the concentration of aggregates of size $i \in \mathbb{N}$. These concentrations are defined in space and time, thus $c_i = c_i(x,t)$, $x \in \Omega \subset \mathbb{R}^3$, $t \in \mathbb{R}^+$. Moreover, we assume a monomer supply and a clearing procedure that reduces each population at a fixed relative rate, then these equations are:

$$\frac{\partial c_i}{\partial t} = \nabla \cdot (\mathbf{D}_i \cdot \nabla c_i) + k_{0,i} - k_{1,i} c_i + N_i + A_i + F_i, \quad i = 1, 2, \ldots,$$

where $\mathbf{D}_i$ denotes the diffusion tensor describing the dispersion of an aggregation of size i, N_i is the nucleation, A_i is the aggregation, and F_i is the fragmentation term. We assume $\nu_{0,1} = \gamma(x)$, $\nu_{0,i} = 0$ for $i > 1$ and $\nu_{1,i} = \nu_{1,i}(x)$. In the context of protein kinetics in NDDs, two different nucleation processes are important. We exclusively investigate binary processes in which the aggregates i and j interact with aggregates of size $i+j$ with an aggregation rate $\nu_{i,j}$ and a fragmentation rate $\beta_{i,j}$ as follows:

$$C_i + C_j \underset{\beta_{i,j}}{\overset{\nu_{i,j}}{\rightleftharpoons}} C_{i+j}, \quad i, j = 1, 2, 3, \ldots.$$

First, the primary nucleation akin to $n_1 > 1$ monomers having an aggregate of size n_1,

$$C_1 + \cdots + C_1 \xrightarrow{\xi_1} C_{n_1},$$

and the secondary nucleation where for $n_2 > 1$ monomers, the existing aggregates allow to form new aggregates [24]

$$C_i + C_1 + \cdots + C_1 \xrightarrow{\xi_2} C_i + C_{n_2}, \quad i = 2, 3, \ldots,$$

where ξ_1 and ξ_2 denote primary and secondary nucleation, respectively. Here, the rate constant with respect to the secondary nucleation is proportional to the overall mass $\sum_{i>1} ic_i$. Considering the above, the nucleation term is given by

$$N_i = \xi_1 \delta_{i,n_1} c_1^{n_1} + \xi_2 \delta_{i,n_2} c_1^{n_2} \sum_{j=2}^{\infty} j c_j, \quad i = 2, 3, \ldots,$$

where, $\delta_{i,j}$ is the Kronecker delta. According to the law of conservation of mass in the nucleation process $N_1 + \sum_{i=2}^{\infty} iN_i = 0$ [24], hence

$$N_1 = -n_1 \xi_1 \delta_{i,n_1} c_1^{n_1} - n_2 \xi_2 \delta_{i,n_2} c_1^{n_2} \sum_{j=2}^{\infty} j c_j.$$

In aggregation process, the aggregate C_i disappears in the presence of C_j to form C_{i+j} (see Fig. 1):

$$C_i + C_j \xrightarrow{\nu_{i,j}} C_{i+j}, \quad j = 1, 2, 3, \ldots, \tag{1}$$

and also appears but with different indices

$$C_{i-j} + C_j \xrightarrow{\nu_{i-j,j}} C_i, \quad j = 1, 2, \ldots, i-1. \tag{2}$$

It is noteworthy that the symmetry produced by exchanging j with $i - j$ in this equation implies that we must count these reactions twice excluding while $i = 2j$. Therefore, these effects can be stated as follows using the law of mass action [46,47]:

$$A_i = \frac{1}{2} \sum_{j=1}^{i-1} \alpha_{j,i-j} c_j c_{i-j} - \sum_{j=1}^{\infty} \alpha_{i,j} c_i c_j,$$

where $\alpha_{i,j} = \alpha_{j,i} = k_{i,j}$, when $i \neq j$ and $\alpha_{i,i} = 2k_{i,i}$, when $i = j$. Consequently, as a result of the double counting, the component $1/2$ appears in the above equation. Finally, the fragmentation terms follow the same dynamics, but they take the reactions (1) and (2) in the reverse direction. Hence, the loss of aggregates C_i is

$$C_i \xrightarrow{\beta_{j,i-j}} C_j + C_{i-j}, \quad j = 1, 2, \ldots, i-1,$$

and the large aggregates create the aggregates of size i by the fragmentation as (see Fig. 1):

$$C_{i+j} \xrightarrow{\beta_{i,j}} C_i + C_j, \quad j = 1, 2, 3, \ldots,$$

results in

$$F_i = -\frac{1}{2} \sum_{j=1}^{i-1} \beta_{j,i-j} c_i + \sum_{j=1}^{\infty} \beta_{i,j} c_{i+j}.$$

The Smoluchowski equations for nucleation-aggregation-fragmentation, taking into account the above equations, can be written as follows [24]:

$$\begin{aligned}\frac{\partial c_i}{\partial t} &= \nabla \cdot (\mathbf{D}_i \cdot \nabla c_i) + \nu_{0,i} - \nu_{1,i} c_i - n_1 \xi_1 \delta_{i,1} c_1^{n_1} - n_2 \xi_2 \delta_{i,1} c_1^{n_2} \sum_{j=2}^{\infty} j c_j \\ &\quad + \xi_1 \delta_{i,n_1} c_1^{n_1} + \xi_2 \delta_{i,n_2} c_1^{n_2} \sum_{j=2}^{\infty} j c_j + \frac{1}{2} \sum_{j=1}^{i-1} (\alpha_{j,i-j} c_j c_{i-j} - \beta_{j,i-j} c_i) \\ &\quad - \sum_{j=1}^{\infty} (\alpha_{i,j} c_i c_j - \beta_{i,j} c_{i+j}), \quad i = 1, 2, \ldots.\end{aligned}$$

The approach discussed here has been used to investigate protein spread in NDDs [24,48].

2.2. Continuous model for disease propagation

Researchers have previously discussed the general aggregation process of different sizes [24,40]. Fornari et al. made many assumptions where the formation and growth of a fibril are dominated at the ends of the fibril by the addition of monomers [24]. As a result, we assume that the fibrils are formed by the addition of monomers. We consider the aggregation process of the form:

$$C_i + C_1 \xrightarrow{\nu_{i,1}} C_{i+1}.$$

We further assume that for polymers, the rates are dependent on size so that the probability of attaching a monomer to a chain depends on the length of the chain, i.e., $\nu_{i,1} = \nu_{1,i} = \nu_{i+1}$ for all $i > 1$, which implies $\alpha_{i,1} = \alpha_{1,i} = \alpha$. Moreover, we will only consider linear aggregation, which has the form:

$$A_i = \alpha(c_1 c_{i-1} - c_i c_1), \quad i = 2, 3, \ldots, N-1,$$

where N is the size of the super particle consisting of all aggregates having a size larger or equal to N. The value of N is determined to be equal to the size of the smallest insoluble particle that does not diffuse and fragment. Thus following [24], c_N is the concentration of a super-particle defined as:

$$\frac{\partial c_N}{\partial t} = -\mu_n c_N + \alpha c_1 c_{N-1}.$$

For the rest of the analysis, we follow [24] and assume that the smallest possible fragment is of size $\zeta = 1$, indicating that the dimer can fragment into two monomers. This is because astrocytes break chains into monomers or clear monomers, even tiny particles. Now the interesting thing about our study is that we can assume that the clearance rate is dependent on the size of the aggregate; in this case, $\nu_{1,i} = \mu_i (i = 1, \ldots, N)$. Here, β_i denotes the fragmentation coming from the astrocytes. In order to incorporate the two factors that contribute to the development of dimers, we make the assumption that nucleation occurs through the generation of dimers by introducing $2\kappa = \alpha_{i,i} + \xi_1$ as shown experimentally [49], where κ represents nucleation. Taking into account the above assumptions, the continuous model is given as follows:

$$\begin{aligned}\frac{\partial c_1}{\partial t} &= \nabla \cdot (\mathbf{D} \cdot \nabla c_1) + \gamma - \mu_1 c_1 - 2c_1^2 \left(\kappa + \xi \sum_{j=2}^{N} j c_j\right) \\ &\quad - c_1 \alpha \sum_{j=2}^{N-1} c_j + \sum_{j=1}^{N-2} \beta_{1+j} c_{1+j}, \\ \frac{\partial c_2}{\partial t} &= 2^{-\eta} \nabla \cdot (\mathbf{D} \cdot \nabla c_2) - \left(\mu_2 + \frac{1}{2}\beta_2\right) c_2 + c_1^2 \left(\kappa + \xi \sum_{j=2}^{N} j c_j\right) \\ &\quad - \alpha c_1 c_2 + \sum_{j=1}^{N-3} \beta_{2+j} c_{2+j},\end{aligned}$$

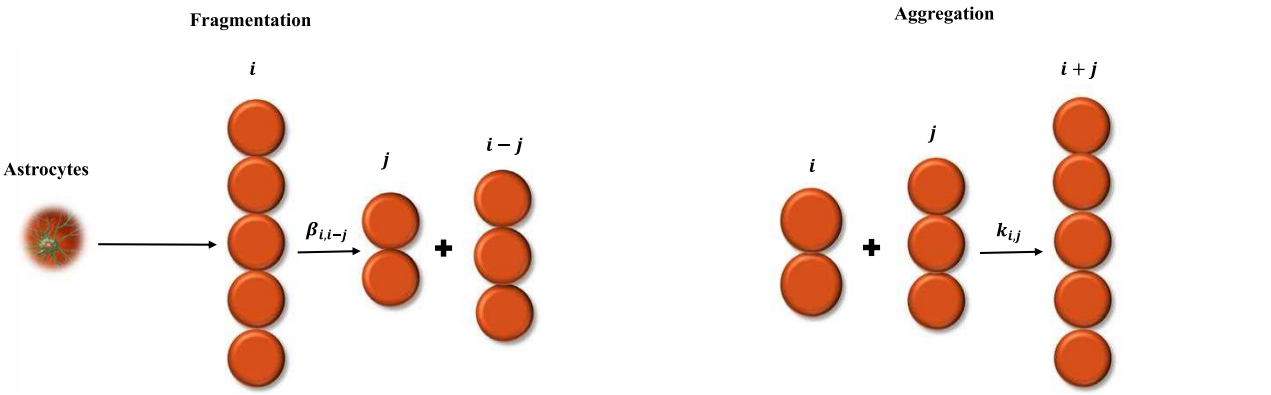

Fig. 1. Fragmentation: this is the process where monomers are created from astrocytes, i.e., an i-mer aggregates with a j-mer to form an $(i-j)$-mer with rate $\beta_{i,i-j}$. Aggregation: this is the process which serves as a good example for the creation of fibrils by adding monomers to an aggregate, i.e., an i-mer merges with a j-mer to form an $(i+j)$-mer with the rate $\nu_{i,j}$.

$$\frac{\partial c_i}{\partial t} = i^{-\eta}\nabla\cdot(\mathbf{D}\cdot\nabla c_i) - \left(\mu_i + \frac{\beta_i}{2}(i-1)\right)c_i + c_1\alpha(c_{i-1} - c_i) + \sum_{j=1}^{N-i-1}\beta_{i+j}c_{i+j}, \quad i = 3,\dots,N-1,$$

$$\frac{\partial c_N}{\partial t} = -\mu_n c_N + \alpha c_1 c_{N-1},$$

where, $\mathbf{D}_i = i^{-\eta}\mathbf{D}$ with $\eta = 1/3$, because different-sized aggregates are transported differently, with larger aggregates diffusing less quickly [50]. The weight of an oligomer is related to its size, and the diffusion coefficient of a soluble molecule scales roughly as a power of its molecular weight [24]. As a result, we use a power law to scale the diffusion tensor according to the size of the aggregates. The relative sizes of the parameters should be taken into account when scaling them properly to create dimensionless new variables. Let m_0 be the total initial mass of the system (or, equivalently, the total initial monomer concentration since we assume constant overall volume). We scale all concentrations with the initial mass m_0 and the time with the usual time associated. The scaling of the variables and dimensionless parameters are then provided by:

$$c_i = m_0\tilde{c}_i,\ t = \frac{1}{m_0}\tilde{t},$$

$$\tilde{\mathbf{D}} = \frac{\mathbf{D}}{m_0},\ \tilde{\gamma} = \frac{\gamma}{m_0^2},\ \tilde{\mu}_i = \frac{\mu_i}{m_0},\ \tilde{\xi} = \xi m_0,\ \tilde{\beta}_j = \frac{1}{m_0}\beta_j.$$

After substitution in the system and then removing the tildes, we obtain

$$\frac{\partial c_1}{\partial t} = \nabla\cdot(\mathbf{D}\cdot\nabla c_1) + \gamma - \mu_1 c_1 - 2c_1^2\left(\kappa + \xi\sum_{j=2}^{N} jc_j\right) - c_1\alpha\sum_{j=2}^{N-1}c_j + \sum_{j=1}^{N-2}\beta_{1+j}c_{1+j}, \tag{3a}$$

$$\frac{\partial c_2}{\partial t} = 2^{-\eta}\nabla\cdot(\mathbf{D}\cdot\nabla c_2) - \left(\mu_2 + \frac{1}{2}\beta_2\right)c_2 + c_1^2\left(\kappa + \xi\sum_{j=2}^{N} jc_j\right) - \alpha c_1 c_2 + \sum_{j=1}^{N-3}\beta_{2+j}c_{2+j}, \tag{3b}$$

$$\frac{\partial c_i}{\partial t} = i^{-\eta}\nabla\cdot(\mathbf{D}\cdot\nabla c_i) - \left(\mu_i + \frac{\beta_i}{2}(i-1)\right)c_i + c_1\alpha(c_{i-1} - c_i) + \sum_{j=1}^{N-i-1}\beta_{i+j}c_{i+j}, \quad i = 3,\dots,N-1, \tag{3c}$$

$$\frac{\partial c_N}{\partial t} = -\mu_n c_N + \alpha c_1 c_{N-1}. \tag{3d}$$

Three significant minor dimensionless parameters ($\beta_i \ll \kappa \ll 1$ and $\xi \ll 1$) are included in this new formulation. As discussed in detail in [24], these parameters are insufficient for a direct simulation of toxic protein evolution in the brain. Consequently, their significance originates from the relative values of a variety of these parameters, which we shall keep in mind throughout our investigation. As a result, in the absence of adequate quantification of these brain parameters, the following study should be regarded as a qualitative examination of solutions rather than quantitative predictions.

3. Large-scale brain network model

It is well known that the neuroanatomical structure of large-scale brain networks offers a skeleton of connected brain regions that promote signalling along preferred paths in support of specific cognitive functions. However, to determine which combinations of interacting brain regions are conceivable, it is necessary to identify the brain areas that compose structural network nodes and the connecting pathways that function as structural network edges [51]. Moreover, the transmission of misfolded proteins from a small infected brain region through axonal fibre pathways across the whole brain is a distinguishing hallmark of prion-like diseases [25]. In the present study, this spreading is modelled as diffusion through the entire brain connectome [52], which is represented as a weighted undirected graph $\wp$ with N nodes and E edges.

3.1. The connectivity-weighted graph

We extract the graph $\wp$ from the tractography of diffusion tensor magnetic resonance images of 1064 healthy subjects of the Human Connectome Project [53] using the Budapest Reference Connectome v3.0 [54]. Further, the connectivity-weighted graph is defined with $N = 1015$ nodes and $E = 16\,280$ edges. The mean fibre number varies between $1 \le n_{ij} \le 4966.5$, with an average of $\bar{n}_{ij} = 39.33$ fibres per edge and most fibres between the superior parietal and the precuneus regions. The mean fibre length varies between 10.270 mm $\le l_{ij} \le$ 83.003 mm, with an average of $\bar{l}_{ij} = 30.089$ mm. The average path length (defined as the average number of steps along the shortest paths for all possible pairs of nodes) and the global clustering coefficient (defined as the

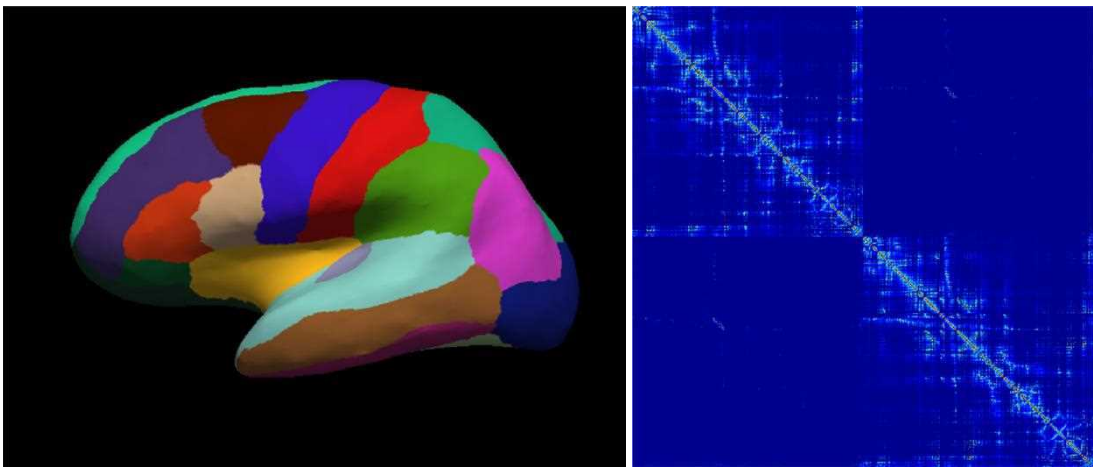

(a) Inflated brain surface (b) The weighted adjacency matrix

Fig. 2. The brain surface is represented by the overall brain regions in the left and right hemispheres. The weighted adjacency matrix with 1015 nodes was obtained by averaging over 418 healthy brains from the Human Connectome Project. Colours represent the connection strength between two regions. Connectivity is moderate to strong within the two brain hemispheres, while there are only a few weak connections between hemispheres.

fraction of paths of length two in the network that are closed over all paths of length two) leads to a small-world network [3] in which highly connected nodes are more likely to become infected and turn into hubs of misfolded protein spreading [24,25].

3.2. The graph Laplacian and Smoluchowski's network model for NDDs

It is noteworthy that the continuous equations for NDDs derived for large N in Section 2 are extremely difficult to integrate over the whole brain, even with the most modern methods. We need to obtain the model by making use of significant anisotropy of the entire network. Therefore, we assume that transport occurs along the axonal tract only, and we substitute the diffusion operator with the graph Laplacian to generate a brain network approximation of the model. We may describe the connectivity of the graph $\wp$ in terms of the weighted adjacency matrix A_{ij} obtained as the ratio of mean fibre number n_{ij} and mean length squared l_{ij} between nodes i and j. From A_{ij}, we compute the weighted degree matrix D_{ii}, a diagonal matrix that characterizes the degree of each node i, and the weighted graph Laplacian L_{ij} as [24]:

$$A_{ij} = \frac{n_{ij}}{l_{ij}^2}, D_{ii} = \sum_{j=1}^{V} A_{ij}, L_{ij} = \rho(D_{ij} - A_{ij}), \quad i,j = 1,\dots,V,$$

where ρ is an overall constant. The inflated view of the whole brain surface obtained from freesurfer is presented in Fig. 2(a). The adjacency matrix is shown in Fig. 2(b). In the present study, the seven brain regions that have been selected are: temporal, parietal, frontal, brain stem and occipital, together with the basal ganglia and the limbic region. We consider each node to be one particular region of the brain. These pronounced variations in degree and adjacency confirm the general notion that the architecture of our brain resembles a small-world network in which highly connected nodes are more likely to become infected and turn into hubs of misfolded protein spreading. Due to transport along the axons across the brain's connectome, we model the spreading of monomers and protein aggregates as a diffusion process. The Smoluchowski network models have been shown to be an excellent approximation of the continuous and discrete brain network model [24]. In this case, we first define $c_{i,j}$ to be the concentration of an aggregate of size i at node j, and the network equations corresponding to the continuous model take the form of a system of $N \times V$ first-order ODEs. Therefore, the network protein model will be:

$$\frac{dc_{1,j}}{dt} = -\sum_{k=1}^{V} L_{jk}c_{1,k} + \gamma_j - \mu_{1,j}c_{1,j} - 2c_{1,j}^2\Big(\kappa_j + \xi\sum_{k=2}^{N} kc_{k,j}\Big) - c_{1,j}\alpha\sum_{k=2}^{N-1} c_{k,j} + \sum_{k=1}^{N-2}\beta_{1+k,j}c_{1+k,j}, \tag{4a}$$

$$\frac{dc_{2,j}}{dt} = -2^{-\eta}\sum_{k=1}^{V} L_{jk}c_{2,k} - \Big(\mu_{2,j} + \frac{1}{2}\beta_{2,j}\Big)c_{2,j} + c_1^2\Big(\kappa_j + \xi\sum_{k=2}^{N} kc_{k,j}\Big) - \alpha c_{1,j}c_{2,j} + \sum_{k=1}^{N-3}\beta_{2+k,j}c_{2+k,j}, \tag{4b}$$

$$\frac{dc_{i,j}}{dt} = -i^{-\eta}\sum_{k=1}^{V} L_{jk}c_{i,k} - \Big(\mu_{i,j} + \frac{\beta_{i,j}}{2}(i-1)\Big)c_{i,j} + \alpha c_{1,j}(c_{i-1,j} - c_{i,j}) + \sum_{k=1}^{N-i-1}\beta_{i+k,j}c_{i+k,j}, \tag{4c}$$

$$\frac{dc_{N,j}}{dt} = -\mu_{n,j}c_{N,j} + \alpha c_{1,j}c_{N-1,j}, \tag{4d}$$

where $i = 3,\dots,N-1$ and $j = 1,\dots,V$. We have also accounted for a possible reliance on clearance and output rates on different nodes.

4. The homogeneous case for the analysis of the $A\beta$ model

In the present section, we will evaluate the total mass of $A\beta$ aggregates when the astrocytic clearance is size-dependent or independent. Also, the analysis of toxic mass has been discussed in detail for three different cases by choosing different parameters for clearance and fragmentation.

4.1. Analysis of total mass

To study in-depth the application of Smoluchowski's modelling framework to our problem, we will find the solutions that are constant in space. Therefore, both the network and continuum

Table 1
Parameter values for the large-scale brain network model for the Aβ [24].

Parameter	Definition	Value
ξ	Secondary nucleation	10^{-3} V
β_i	Fragmentation rate	As given in Section 4.2
α	Elongation rate	1
γ	Production rate	10^{-2} V^2
μ_i	Clearance rate	As given in Section 4.2
ρ	Diffusion constant	2×10^{-5}
m_0	Initial monomer c	1
V	Number of nodes	1015
N	Super particle size	400

models have the same set of ordinary differential equations given as follows:

$$\frac{dc_i}{dt} = \gamma\delta_{1,0} - \mu_i c_i + N_i + A_i + F_i, \quad i = 1, 2, \ldots, N-1,$$

$$\frac{dc_N}{dt} = -\mu_N c_N + c_1 c_{N-1},$$

where the relevant parameters are given in Table 1, and they take values according to different cases given in Section 4.2. Moreover, $\kappa_i = 10^{-3}(\sum \delta_{i,j})$, where $j = 190$ to 198 and $j = 698$ to 706, is defined as the nucleation at node i corresponding to the posterior cingulate region of the brain for our integrated data. The total mass and the total number of aggregates are given by:

$$P_{tot} = \sum_{i=1}^{N} c_i, M_{tot} = \sum_{i=1}^{N} i c_i.$$

The total mass is not conserved if $N \to \infty$ [46]. Although, for finite N, the evolution of mass is given by

$$\frac{dM_{tot}}{dt} = \gamma - \sum_{i=1}^{N} i\mu_i c_i.$$

If clearance is independent of size, we have $\mu_i = \mu$, therefore

$$\frac{dM_{tot}}{dt} = \gamma - \mu M_{tot},$$

the initial conditions at time $t = 0$ are $M_{tot}(0) = c_1(0) = 1 = \gamma/\mu$. Further, the whole mass is then conserved and stable (against small perturbations of the initial state), i.e., $M_{tot} = 1$ as a result of the scaling option. Starting with a monomer population of $c_1(0)$, the total mass stays constant while aggregates are formed at the cost of the monomer population. As long as gelation does not occur, this process is independent of the aggregation mechanism. Gelation is similar to treating the super-particle independently in a finite system. Because the net flow to the super-particle is limited, the mass of some other aggregates is transferred to the super-particle. Moreover, if clearance is dependent on size, we have $\mu_i = \mu/i$, then

$$\frac{dM_{tot}}{dt} = \gamma - \mu P_{tot},$$

again the initial conditions at time $t = 0$ are $M_{tot}(0) = c_1(0) = 1 = \gamma/\mu$. Since $P_{tot} \leq M_{tot}$ and the equality happens only if $M_{tot} = P_{tot} = c_1$, we get $M_{tot} > \gamma - \mu P_{tot} > 0$ for $t > 0$ and the overall mass of the system increases due to the formation of additional monomers. Particles belonging to aggregates are removed from the system through clearing, although their removal is slower than monomer removal. More formally, if we have $\mu_i \leq \mu_1, \forall i > 1$, and at least one $k > 1$ such that $\mu_k \leq \mu_1$, then, using the same reasoning and initial conditions, we have $M > 0$ for $t > 0$. Also, the system's total mass increases in this case.

4.2. Analysis of toxic mass

According to our model, for the remainder of the homogeneous system analysis for $A\beta$ model, we will study four different cases. We assume that N is high enough not to alter the dynamics on intermediate time scales of disease progression. Hence, it is appropriate to investigate the system in the limit $N \to \infty$. Furthermore, we are looking for the solutions with no initial seeding, where $c_1(0) = 1$, and $c_i(0) = 0, i > 1$. As a result of the system, we have $c_1(t) \in [0, 1]$ and the total mass $M(t) \in [0, 1]$ at all times (where $M = \sum_{i=1}^{\infty} i c_i$). The homogeneous system now reads:

$$\frac{dc_1}{dt} = \gamma - \mu_1 c_1 - 2c_1^2\left(\kappa_j + \xi \sum_{k=2}^{\infty} k c_k\right) - c_1\alpha \sum_{k=2}^{\infty} c_k + \sum_{k=1}^{\infty} \beta_{1+k} c_{1+k},$$

$$\frac{dc_2}{dt} = -\left(\mu_2 + \frac{1}{2}\beta_2\right)c_2 + c_1^2\left(\kappa_j + \xi \sum_{k=2}^{\infty} k c_k\right) - \alpha c_1 c_2 + \sum_{k=1}^{\infty} \beta_{2+k} c_{2+k},$$

$$\frac{dc_i}{dt} = -\left(\mu_i + \frac{\beta_i}{2}(i-1)\right)c_i + \alpha c_1(c_{i-1} - c_i) + \sum_{k=1}^{\infty} \beta_{i+k} c_{i+k},$$

where c_i $(i \geq 1)$ represents the concentrations of $A\beta$. Note that the production rate is $\gamma = 10^{-2}$ for all cases to analyse the toxic mass. While the primary nucleation process is required to produce initially toxic seeds, various proteins have unique expansion mechanisms (secondary nucleation or fragmentation). In vitro experiments on the formation of oligomers based on the Aβ peptide have shown [24,55] that both primary and secondary nucleation processes are required to capture the kinetics of the process across different initial concentrations correctly. Through a positive feedback process, once a population of toxic seeds has been created and grown, it acts as a catalyst for developing new seeds. The value of μ has been explicitly started with 0.001. Let us discuss three different cases, where we choose different parameters for each case as follows:

- Case I: $\mu_i = \mu, \alpha = 1, \beta_i = 0$;
- Case II: $\mu_i = \frac{\mu}{i}, \alpha = 1, \beta_i = 0$;
- Case III: $\mu_i = \mu, \alpha = 1, \beta_i = \frac{0.01}{i}$.

4.2.1. Case I

In the present case, we assume that $\mu_i = \mu, \alpha = 1$ and $\beta = 0$ (i.e., no fragmentation) for the continuous model (Eqs. (3)), then we get the trivial model as given in [24]. The graph presented in Fig. 3(a) is similar to the one obtained in [24].

4.2.2. Case II

In this section, first, we assume that the clearance rate depends on the aggregate size. In this case of size-dependent distribution, the clearance is $\nu_{1,i} = \mu_i$ for $i = 1, \ldots, N$. Second, we may assume that the clearance of an oligomer with i-element is the same as the elimination of each element for a certain phagocytic activity or antibody. As a result, chains of size N or greater cannot be removed, and the removal of large chains becomes progressively difficult. Also, size-dependent clearance rates are inversely proportional to oligomer size that is $\mu_i = \frac{\mu}{i}$ for $i = 1, \ldots, N-1$, the growth parameter α remains constant. Finally, we assume that there is no fragmentation, then Aβ and τ protein aggregates grow into increasingly larger fibrillar assemblies, and the parameters we selected for the present case are as follows:

$$\mu_i = \frac{\mu}{i}, \alpha = 1, \beta_i = 0.$$

Because τ is an intracellular protein, these large aggregates spread predominantly through the network of axonal pathways. Similarly, Aβ is known to produce large extracellular aggregates.

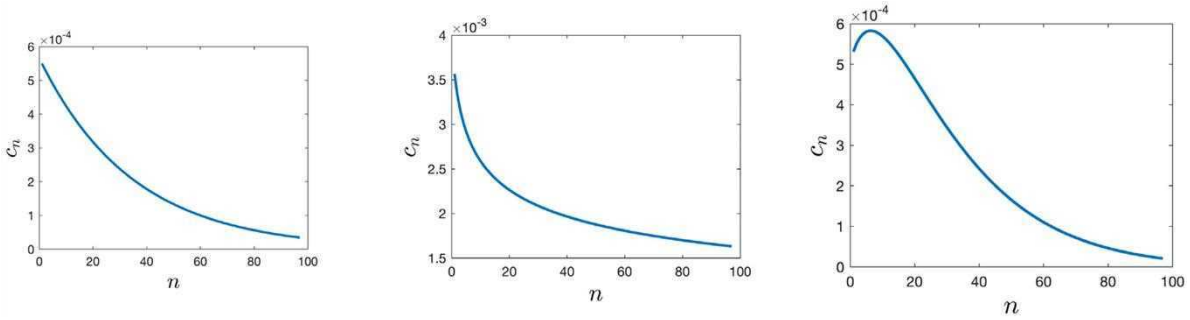

(a) Case I (b) Case II (c) Case III

Fig. 3. The asymptotic size-dependent distribution of the homogeneous Aβ model for three cases (a)–(c).

Assuming that these aggregates are moved inside the brain via a simple diffusion process, diffusion tensor imaging shows that diffusion occurs preferentially along the axons [24]. As a result, although these proteins are located outside the cell, they also diffuse anisotropically. It is well known that astrocytes play an important role in the clearance of Aβ [56]. An approach having such procedures, where astrocytes clear Aβ are now being discussed [57,58]. Importantly, as depicted in Fig. 3(b), initially in the healthy brain astrocytes function as supporting cells to contribute to immunity and maintain the ionic homeostasis of the CNS. When the activation of astrocytes is moderate, they protect neurons and promote an increase in Aβ. In the presence of AD, the aggregates reach a peak value and astrocytes are activated [59–61]. Since astrocytes interact with each other and there is much association between astroglia, activation of one type would cause activation of the other [27]. These toxic changes lead to a threshold, and the concentrations of aggregates in the brain destroy the healthy balance, as can be seen in Fig. 3(b). Finally, as the level of Aβ reaches a peak point, there is a rapid spread of τ in the whole brain. Since there is no fragmentation, astrocytes cannot clear Aβ. Furthermore, when there is enough Aβ, astrocytes in the AD brain lose their capacity to regulate their ionic equilibrium, particularly about the generation of excess glutamate, producing an increase in its neurotoxic effects, inhibition of astroglia phagocytosis by increasing its activation. Astrocyte activation causes neuronal injury by releasing potentially harmful chemicals such as proinflammatory cytokines, reactive oxygen intermediates, proteinases, and complement proteins [58]. Our findings show that astrocytes in the absence of fragmentation have the biggest influence on Aβ during the seeding stage, most likely by disrupting Aβ clearance and increasing Aβ aggregation [27].

4.2.3. Case III

In the present case, we assume that the clearance rate is independent of the size of the aggregates. We also consider that the fragmentation depends on the size of aggregates given as follows:

$$\mu_i = \mu, \alpha = 1, \beta_i = \frac{0.01}{i}.$$

Now in the presence of fragmentation, Aβ and τ protein aggregates become more toxic [62]. These fragments contain important regions of the full Aβ and τ proteins, and Aβ is an amphipathic peptide with similar aggregation tendency and toxicity [63]. We found that when the capacity of early Aβ oligomers tries to bind τ monomers, one potential cause of toxicity is the reduction of the *tau* population that is needed to regulate the dynamics of astrocytes. Other potential toxicity routes can be found in the structures of heteroligomers generated by the contacts of various τ to Aβ fragments, which need to be investigated more thoroughly [63]. During the fragmentation, the transportation of monomeric, oligomeric, and fibrillar particles activate astrocytes, which causes the progression of AD throughout the brain.

In this case of size-independent clearance, we notice that in the presence of Aβ, for new developmental stages, fragmentation generates new seeds from larger aggregates. These new seeds from larger aggregates create new targets for monomers to be transformed into toxic proteins. The results are presented in Fig. 3(c). We note that this size distribution is markedly different than the one found for $\beta = 0$ in Case II. In Fig. 3(c), it is shown that the fragmentation clears monomers initially and breaks chains even for the smallest particles of size i into monomers. The initial dynamics are dominated by the nucleation process since the fragmentation comes from astrocytes. Here, astrocytes play an important role in the presence of Aβ and τ protein aggregates, which may act as both neuroprotective and neurotoxic cells. In the initial stages of AD, the activated astroglia show neuroprotective behaviour. However, when AD progresses, these glial cells become overactivated, resulting in neurotoxic functionality. Since glial cells interact with each other, there is a loop of overactivation and activation occurring within the glial population [27]. As depicted in Fig. 3(c), the decline phase in the size distribution of aggregates provides useful information if the fragmentation is size-dependent. We see that when the effect of Aβ has reached its limit, which means that there is no further increase in Aβ, Fig. 3(c) shows that activated and overactivated astrocyte populations continue to increase with time. This trend is in agreement with experiment [64]. It suggests that limiting AD to the effects of Aβ alone is inaccurate and that the importance of τ proteins, clearance rate of monomers, and astrocyte neuroinflammation must be included when studying the etiology of AD. Furthermore, the findings demonstrate that increasing monomer clearance, as well as any therapeutic therapy that deactivates astrocytes, slows the progression of AD.

5. Large-scale brain network simulation

In the present section, we consider the dynamic analysis of protein concentrations at the network level. Among other challenges, we are motivated by the quests of (a) how the clearance mechanisms can be modelled and (b) how changes in the clearance or aggregation processes affect the system's stability to aggregation pertaining to the specific homogeneous case to the ones on the entire brain network. These are two important unanswered questions in the field of neurodegeneration. Here, we generalize existing protein aggregation models to account for both the synthesis of monomers and the removal of protein aggregates. We demonstrate that, given the specifics of the clearance effects, a critical clearance value occurs at which aggregate accumulation is prohibited. Our findings demonstrate that a sudden change from a healthy to a diseased state can be attributed

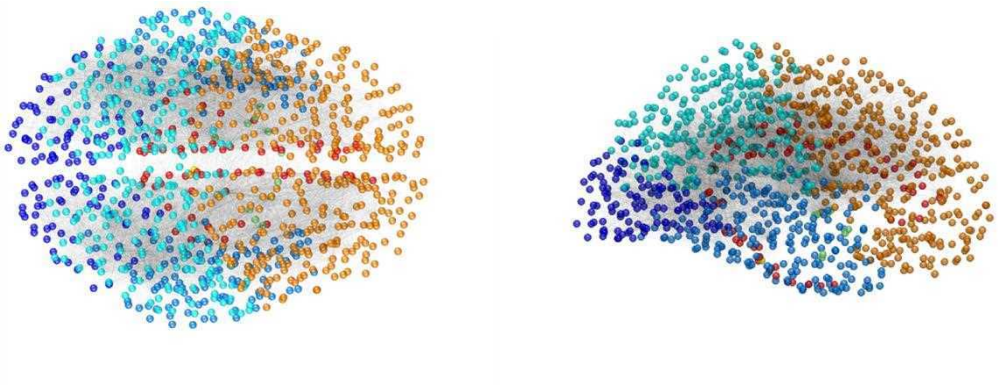

(a) Longitudinal view of brain (b) Sagittal view of brain

Fig. 4. Three-dimensional views of the brain with its seven associated regions (the different colour nodes associated with each brain region are the same as the legends presented in Fig. 6(b)).

to small variations in the effectiveness of the clearance process. Additionally, they offer a mathematical framework for investigating the specific impacts of various clearance mechanisms on the accumulation of aggregates in the case described in the previous Section 4. While the entire brain is a highly heterogeneous system, classical diffusion is better suited for modelling the free movement of aggregates in a homogeneous medium when it comes to large-scale brain networks. Prions would spread equally quickly in all spatial directions if diffusion in a homogeneous medium were to be modelled. As prions propagate through neural pathways, where disease may reach distant brain regions simultaneously or even faster than neighbouring regions, this is unlikely to occur in practice [48]. Network nodes are divided into susceptible and infected nodes; susceptible nodes catch the disease if at least one of their linked neighbours does. Hence, the network approach models a fast disease spread inside clusters of highly connected neurons and propagation to additional clusters via long-distance connections, in contrast to a homogeneous diffusional spread.

Since the whole brain is considered a network, from one node to the complete network, we validate the scale parameters and homogeneous equations. Let m_0 be the total mass of the monomer, assumed to be spread evenly across all V nodes, and the initial conditions for the entire network are

$$c_{1,j} = 1/V, c_{k,j} = 0, k = 2, \ldots, N; j = 1, \ldots, V.$$

Then, for the network to have the same kinetics as the homogeneous system, we must scale the variables as $c = c_h/V$ and parameters from the homogeneous system (now described by the subscripts "h") as follows: $\gamma = \gamma_h/V^2, \mu = \mu_h/V, \xi = \xi_h V, \beta = \beta_h/V, \kappa = \kappa_h$. Similarly, the time scale is now $t = t_h V$. Considering the homogeneous case discussed in the previous section, for the network to have the equivalence kinetics, we set $\kappa_i = \kappa$ and $\rho = 0$ in Eqs. (4). Therefore, the population of toxic proteins has the same dynamics as shown in Fig. 3 for each case. The important thing is how to correctly seed the system to demonstrate that the disease begins in a certain region. We can either start with a non-zero initial condition of oligomers at a particular node or assume that nucleation is the primary mechanism for the initial creation of toxic proteins at a given node. In this case, we use the latter modelling assumption and suppose that κ_i vanishes everywhere except at certain nodes where it has a small value. These nodes are recognized to be the seeding sites for NDDs (the list of regions of interest, together with their node number, lobe, hemisphere, and spatial coordinates is given in the supplementary material of Ref. [24]). The views of the brain with its seven associated regions are shown in Fig. 4.

5.1. Analysis of Aβ toxic protein mass and total monomers

It is noteworthy that the overall toxic mass (obtained by adding the masses of all aggregates at each node) evolves in a similar manner as for a homogeneous system, although the system is not homogeneous.

5.2. Spreading behaviour

A biomarker is a global metric used to characterize the progression of neurodegeneration throughout the brain [25,65]. The biomarker abnormality is calculated as the temporal evolution of the total concentration of misfolded proteins integrated across a specific region of interest or the entire brain. We consider the biomarker spectrum of the toxic proteins of the size distribution to illustrate the dynamics of the Smoluchowski model. Over the entire brain network, to better understand the development of toxic proteins, we compute the toxic mass as a function of time at each node:

$$M_j(t) = \sum_{i=2}^{N} c_{i,j}(t), \quad j = 1, \ldots, V.$$

We average the toxic mass of all regions considered in the present study, e.g. the usual four lobes: basal ganglia, temporal, parietal, frontal occipital along with the limbic region, basal ganglia and brain stem as shown in Fig. 4. The average formula is:

$$M^{(j)} = \frac{1}{x_j} \sum_{i \in X_j} M_i, \quad j = 1, \ldots, 7,$$

where X_j is defined as the set of all nodes in that region and x_j is the number of elements of X_j. The development of the toxic mass at each node clearly shows the additional delay in disease progression caused by diffusion from one node to the next. While the disease progresses quickly at the seeded node, additional nodes experience the disease on a new time scale that is directly related to diffusion (via the overall scaling constant). The frontal pole, located at the extreme of the frontal lobe and sparsely linked in the connectome, is the final node to be invaded. The occipital lobe becomes the final lobe to be infected if these extreme nodes are omitted from the calculation. Since we discussed three different cases in detail in the previous Section, now we will study those cases over the entire brain network with 1015 nodes and seven selected regions.

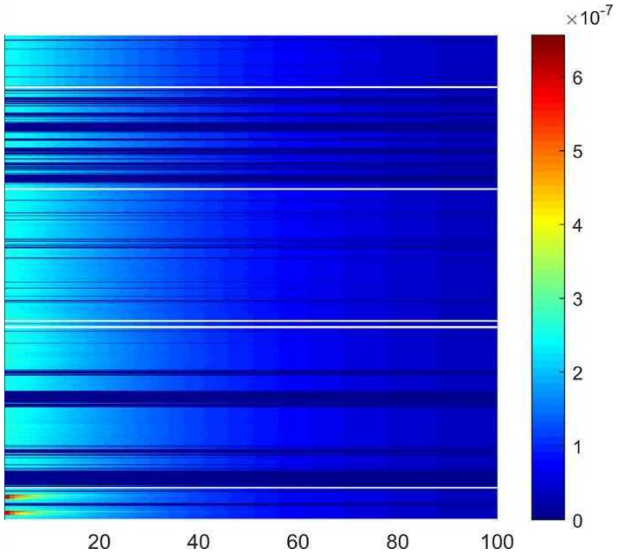

Fig. 5. Spreading behaviour of toxic proteins Aβ over the entire brain network for Case I. Here, the x-axis (left to right) represents n monomers and the y-axis (from bottom to top) represents the following brain regions, respectively: limbic, frontal, basal ganglia, parietal, temporal, occipital and brain stem.

As presented in Fig. 5, we see that for Case I, when there is no fragmentation, the node curves do not intersect, this means that the order of the nodes by the toxic mass does not considerably alter [24]. The progression of the disease state can be seen region-wise over the whole brain in Fig. 5. Although, the brain stem is not visible in Fig. 5 because it contains only one node and white lines represent the separation of regions. We observed that in Fig. 5, initially, the system only significantly changed from having a massive population of healthy monomers to dimers and the seeded nodes are the only nodes that are affected. This behaviour can be seen in Fig. 5, where the seed's concentration is observed to rise linearly before affecting additional nodes. Later, depending on the kinetics, the toxic mass at the seeded node increases. It also expands at additional nodes. Here, the nodes that are directly related to the seeding nodes will undergo the primary infection. The network structure and protein kinetics affect the secondary infection. Only areas around the nodes connecting to the seeding nodes are affected. Following the secondary infection, the infection of the entire system progresses fast and reaches the brain stem. Only sparsely linked nodes, such as the limbic, and frontal poles, are less affected.

Previously, we have discussed the temporal dynamics of Case II in detail in Section 4.2.2. Now we will see the spreading behaviour of toxic proteins over the entire brain network when the clearance is size-dependent and fragmentation is zero in Fig. 6. Moreover, over the nodes, the curves do not intersect and the toxicity does not alter. However, in the absence of fragmentation Aβ and τ protein aggregates develop into larger and bigger fibril assemblies. These large aggregates mostly disperse across the brain network of axonal routes since τ is an intracellular protein. Through diffusion, when the large aggregates move from extracellular to intracellular space in the brain nodes the disease state occurs. Importantly, now the clearance is size-dependent as astrocytes help to clear all the monomers, even the smallest one until the toxic mass changes reach a threshold. The astrocytes clear all the monomers until the toxicity increases and seeded nodes converge to a disease state. It can be seen that in Fig. 6(a), the seeded nodes in specific regions have a strong connection between them, so at the later stage, all the nodes are infected over the whole brain. It is depicted in Fig. 6(a) that the toxicity spreads over the whole brain when the nodes intersect with each other. Moreover, as presented in Fig. 6(a), the time scale we have chosen is large which is why we see that all the nodes converge to a disease state. If we take a small time scale, the behaviour of toxic mass at each node will be the same as presented in Fig. 8(a). We have presented the zoom view of toxic mass at each node as shown in the insert of Fig. 6(a). Importantly, we assume that the smallest possible fragment is of size $\zeta = 1$, implying that once a dimer is produced, it remains stable and does not fragment. Aggregation must be preferred over fragmentation, i.e., $\beta < \alpha$ to create large aggregates. The evolution of fibril length, the transfer from tiny aggregates to larger aggregates, is referred to as growth. Growth increases the size of a toxic seed once it has been generated. Later on, either fragmentation or clearance of monomers diminishes this process. As shown in Fig. 6(a), the dynamic is related to many spatio-temporal scales.

Initially, the toxic protein population grows exponentially over a typical time scale calculated by assuming that $m(t) = c_1(t) = 1$. However, when compared to the amount of toxic protein, the size distribution only approaches its asymptotic value over a significantly longer average time scale. Now, the astrocytes help to clear all the monomers, even the smallest particles. In AD, each monomer's self-assembly process is affected by the two fragments, Aβ plaques and τ proteins [63]. The τ protein has a strong preference for forming heteroligomers with other Aβ monomers and oligomers. Whether the population of Aβ or τ is dominant, it determines the configurations and properties of the heteroligomers. The addition of τ to rich Aβ oligomers reduces Aβ aggregation tendency but does not eliminate fibril formation. The τ monomers and dimers, on the other hand, can progress to bigger oligomers and form granular aggregates by forming complexes with Aβ. These heteroligomers may contribute to toxicity by disrupting τ normal function or by causing the aggregates to be toxic. It can be seen clearly in Fig. 6(b), initially, the spreading behaviour in the specific regions is increasing. The seeded nodes will spread infection in the connected nodes as opposed to the kinetics of aggregation. It is evident that the majority of nodes in the specific regions become infected fast at this stage. At this time, the disease has spread to all nodes in each region, and the toxic mass quickly achieves its peak value in homeostasis with the mass of healthy monomers. The most affected nodes are occipital and parietal, as presented in Fig. 6.

Next, Fig. 7 represents the distribution of disease over the entire brain network by averaging the toxic mass at each node and in the specific regions. Importantly, by bringing aggregates from adjacent areas to the local area, diffusion has the impact of lowering local concentrations that are high. Diffusion enables seeds to spread since it starts in a specific, concentrated, small region. In Fig. 7, the progression of the toxic mass at each node clearly illustrates the additional delay in disease propagation imposed by diffusion from one node to the next. While the disease spreads quickly at the seeding node, it affects additional nodes on a new time scale that is directly related to diffusion (through the overall scaling constant ρ). It is depicted in Fig. 7 that the spatio-temporal patterns of n monomers over the brain regions such as limbic, frontal, basal ganglia, parietal, temporal, occipital and brain stem show that these regions are directly relevant to the disease progression. The local dynamics of brain regions are displayed vertically (from bottom to top) and begin with seeding before progressing through growth, expansion, and saturation. In Fig. 7, the limbic region that is most damaged in this situation is represented by the area that is extremely red and dense. Given that the limbic area is located in the middle of the brain, the likelihood of disease progression is increased. Since the clearance is size dependent, initially the toxic mass increases linearly.

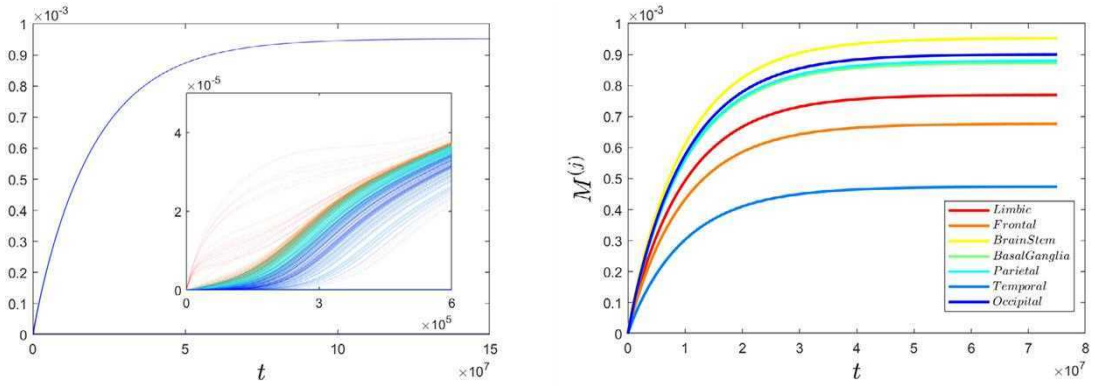

(a) Toxic mass at each node $M_j(t)$

(b) Average toxic mass for each region $M^{(j)}$

Fig. 6. Spreading behaviour of Aβ toxic proteins over the entire brain network for Case II.

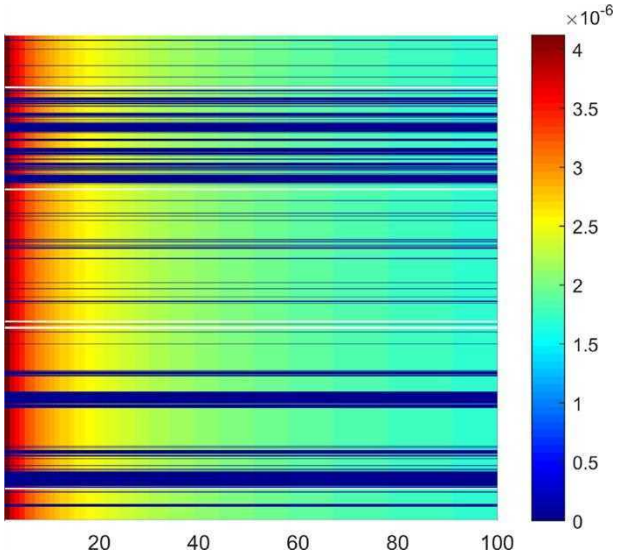

Fig. 7. Distribution of disease over the entire brain network for Case II. x-axis(left to right) represents n Aβ monomers and y-axis (from bottom to top) represent the following brain regions, respectively: limbic, frontal, brain stem, basal ganglia, parietal, temporal, and occipital.

Later on, clearance slows down the progression of the disease. Importantly, in the absence of fragmentation, astrocytes will not clear Aβ, but it is well acknowledged that clearance is essential for slowing the progression of AD. To the best of our knowledge, these are the novel results so far for the spatio-temporal dynamics of Smoluchowski's model for NDDs. Our prediction is accurate in the sense that clearance varies with the aggregate size and is key to slowing down the progression of the disease [24,25,28]. Considering Case III, when the clearance rate is independent of the size of the aggregates, and the fragmentation is non-zero, astrocytes help to clear all the monomers, initially. We see that in Fig. 8(a), the activated and overactivated astrocyte populations e.g., the toxic mass increased until all the nodes intersect and the toxicity spreads over the whole brain. Although astrocytes help to clear even the smallest particle since the fragmentation is size dependent and the clearance rate is constant, the Aβ and τ proteins become more toxic, this would result in a higher concentration of toxic mass as shown in Fig. 8(b). Finally, the disease starts and the basic infection occurs in nodes associated with the seeded nodes and is primarily governed by the diffusion process as opposed to the kinetics of aggregation. These nodes reproduce new seeds, which causes the secondary infection in all nodes associated with the original nodes, and so on. Given that the average path length is around 1.5 cm^2, it is obvious that this network layout causes most nodes to become infected quickly at this stage. The disease has spread to all nodes at this point, and the toxic mass soon reaches its maximum values in equilibrium with the mass of healthy monomers.

Next, let us discuss the distribution of disease over the entire brain network for Case III, as shown in Fig. 9. We see that in Fig. 9(a), the distribution of disease on brain nodes, where the dark red part is highly affected, and less red is less affected. Moreover, the spatio-temporal patterns for Case III are represented in Fig. 9(b), and we see the disease distribution of n monomers over the brain region such as limbic, frontal, basal ganglia, parietal, temporal, occipital and brain stem. The highly red dense part represents the limbic region that is most affected in the present case. Since the limbic region is found in the middle portion of the brain, there are higher chances of disease progression. The consequence of fragmentation is the development of smaller aggregates, which not only accelerates clearance but also increases the total expansion of the protein population. We anticipate a decrease in the critical value of clearance as well as the potential of a limited value of clearance since smaller aggregates are more likely to be cleared. Importantly, the choice of clearance rates certainly has a big influence on clearing values since they vary from the smallest to the highest [66]. Therefore, the total rise in aggregate mass in the present case may depend greatly on whether the clearance process is enhanced or inhibited. Since the clearance rate is constant the monomer's production increases. Therefore, this model for Case III maintains the total initial mass of the monomers when clearance is independent of aggregate size.

Our data contains 1015 nodes, and we divide our job into many processors. We have selected the number of CPUs as the divisors of 1015. Like, for 10,000 iterations, for 1 CPU, the computational time is 4398.6 s, for 5 CPU's it is 120.06 s, for 7 CPU's, it is 89.46 s, and for 35 CPU's, it is 30.67 s. If we solve the problem using standard serial programming, this requires a significant

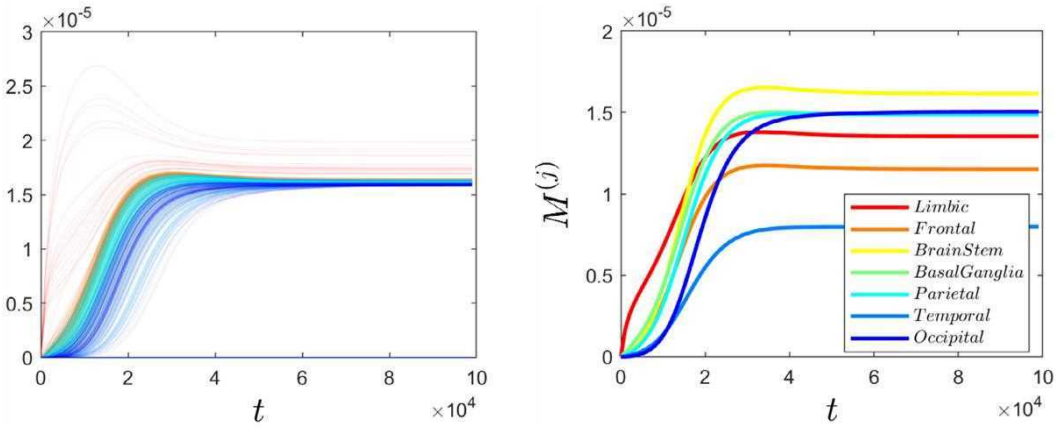

(a) Toxic mass at each node $M_j(t)$ (b) Average toxic mass for each region $M^{(j)}$

Fig. 8. Spreading behaviour of Aβ toxic proteins over the entire brain network for Case III.

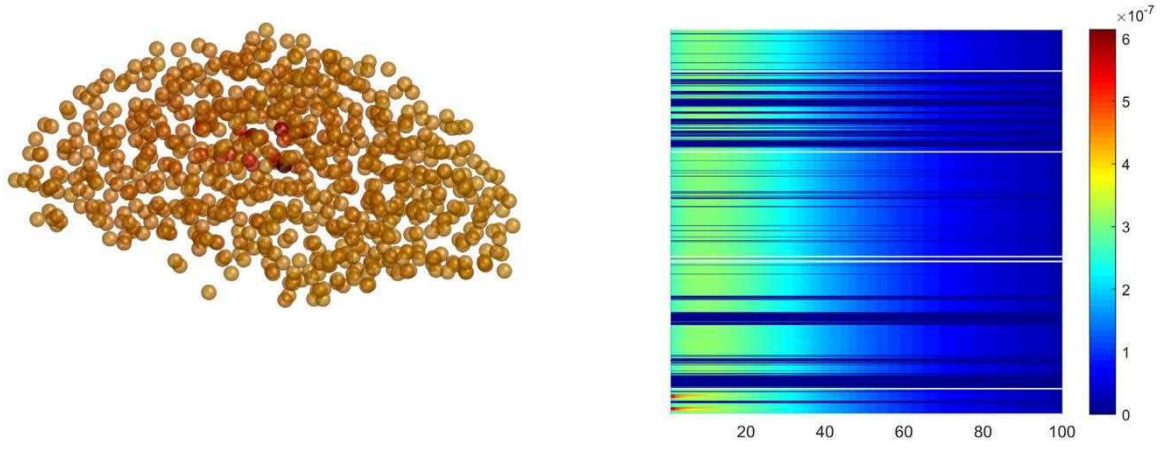

(a) (b)

Fig. 9. Distribution of disease over the entire brain network for Case III. (a) Average toxic mass of Aβ at each node. (b) the x-axis (left to right) represents n-monomers and the y-axis (from bottom to top) represents the following brain regions, respectively: limbic, frontal, brain stem, basal ganglia, parietal, temporal, and occipital.

amount of computing time. Through the use of open MPI and the C programming language, we can reduce computing time. We divide the sequential tasks involving the spatial points among available processors for each time iteration and perform them in parallel. All figures have been plotted and shown in Matlab after the data have undergone post-processing. To reduce the time required to acquire results for the parallel computation, we employed the SHARCNET supercomputer facilities.

6. Conclusions

According to the prion-like hypothesis of neurodegenerative diseases (NDDs), the concentration of misfolded proteins causes tissue death, neurodegenerative pathology, and cognitive decline. The present study has focused on developing a modified multi-scale brain network model and analysing dynamic processes in studying the properties of important NDDs, for instance, AD. The concentration of proteins is in the form of aggregates and since these aggregates are of various sizes and have various transport properties and toxicity, it is crucial to track their evolution independently over time and space. The growth of the aggregates is taken into account as a continuum with diffusion along axonal routes and the model takes the form of sets of nonlinear Smoluchowski equations interacting on a network through the graph Laplacian.

In the present study, we have considered the Smoluchowski model to study the spread of intracellular protein aggregates along with astrocytes across the brain. Here, we considered three paradigmatic cases for the intracellular spread of τ molecules where fragmentation is important and for the extracellular dispersal of $A\beta$, which is further increased by secondary seeding and aggregation. The interesting finding of our study is that when the clearance depends on the aggregate size, these multi-scale brain network models will not conserve the total initial mass of monomers. As a result, the usual qualitative traits of toxic proteins identified through brain regions and nodes are persistent and closely related to the development of the disease over the brain network. Fragmentation comes from astrocytes, and it is essential for seeding a non-monotonic distribution of aggregate concentrations. The accumulation of misfolded $A\beta$ in the brain is thought to be the result of an imbalance in its production and clearance. We found that the astrocytes play an important role in clearing $A\beta$ even for the smallest possible fragment of size $\zeta = 1$. Importantly, in our work, we have used the astrocytic clearance for the $A\beta$, and we assume that astrocytes do not clear the

toxic τ proteins. Our results are consistent with the experimental studies [67–71]. The proposed novel model is sufficiently flexible to be further adapted to more complex dynamics or connected to other important phenomena according to the theory described here. It is well known that clearance is essential for stopping the progression of AD. Therefore, to understand fundamental mechanisms and pinpoint potential treatment targets, it will be essential to further carefully study the related parameters and their connections to other phenomena associated with the progression of AD. Finally, we predicted that when fragmentation does not depend on the aggregate size, astrocytes help to clear the initial mass of monomers. Hence, it will be interesting for future studies to critically address the ways in which fragmentation varies with the aggregate size, which would greatly facilitate the research and comprehensive analysis of the standard model.

CRediT authorship contribution statement

Hina Shaheen: Conceived and designed the analysis, Collected the data, Contributed data or analysis tools, Performed the analysis, Wrote the paper. **Swadesh Pal:** Conceived and designed the analysis, Contributed data or analysis tools, Supervision, Concept, Review. **Roderick Melnik:** Conceived and designed the analysis, Supervision, Concept, Review.

Declaration of competing interest

The authors declare that they have no known competing financial interests or personal relationships that could have appeared to influence the work reported in this paper.

Data availability

Data will be made available on request.

Acknowledgements

The authors are grateful to the NSERC, Canada and the CRC Program, Canada for their support. RM is also acknowledging the support of the BERC 2022–2025 program and the Spanish Ministry of Science, Innovation and Universities through the Agencia Estatal de Investigacion (AEI) BCAM Severo Ochoa excellence accreditation, Spain SEV-2017–0718. This research was enabled in part by support provided by SHARCNET, Canada (www.sharcnet.ca) and Digital Research Alliance of Canada (www.alliancecan.ca).

References

[1] R.F. Betzel, D.S. Bassett, Multi-scale brain networks, Neuroimage 160 (2017) 73–83.
[2] A. Fornito, A. Zalesky, E. Bullmore, Fundamentals of Brain Network Analysis, Academic Press, 2016.
[3] D.S. Bassett, E. Bullmore, Small-world brain networks, Neuroscientist 12 (6) (2006) 512–523.
[4] E.T. Bullmore, D.S. Bassett, Brain graphs: graphical models of the human brain connectome, Annu. Rev. Clin. Psychol. 7 (2011) 113–140.
[5] O. Sporns, The human connectome: a complex network, Ann. New York Acad. Sci. 1224 (1) (2011) 109–125.
[6] H.-J. Park, K. Friston, Structural and functional brain networks: from connections to cognition, Science 342 (6158) (2013) 1238411.
[7] A. Vosoughi, S. Sadigh-Eteghad, M. Ghorbani, S. Shahmorad, M. Farhoudi, M.A. Rafi, Y. Omidi, Mathematical models to shed light on amyloid-beta and tau protein dependent pathologies in Alzheimer's disease, Neuroscience 424 (2020) 45–57.
[8] M. Andjelković, B. Tadić, R. Melnik, The topology of higher-order complexes associated with brain hubs in human connectomes, Sci. Rep. 10 (17320) (2020) 1–10.
[9] A.M. Fjell, M.H. Sneve, A.B. Storsve, H. Grydeland, A. Yendiki, K.B. Walhovd, Brain events underlying episodic memory changes in aging: a longitudinal investigation of structural and functional connectivity, Cerebral Cortex 26 (3) (2016) 1272–1286.
[10] A.M. Fjell, M.H. Sneve, H. Grydeland, A.B. Storsve, I.K. Amlien, A. Yendiki, K.B. Walhovd, Relationship between structural and functional connectivity change across the adult lifespan: a longitudinal investigation, Hum. Brain Mapp. 38 (1) (2017) 561–573.
[11] J. Zimmermann, P. Ritter, K. Shen, S. Rothmeier, M. Schirner, A.R. McIntosh, Structural architecture supports functional organization in the human aging brain at a regionwise and network level, Hum. Brain Mapp. 37 (7) (2016) 2645–2661.
[12] J. Faskowitz, R.F. Betzel, O. Sporns, Edges in brain networks: Contributions to models of structure and function, Netw. Neurosci. 6 (1) (2022) 1–28.
[13] J.M. Shine, E.J. Müller, B. Munn, J. Cabral, R.J. Moran, M. Breakspear, Computational models link cellular mechanisms of neuromodulation to large-scale neural dynamics, Nature Neurosci. 24 (6) (2021) 765–776.
[14] A. Fornito, A. Zalesky, M. Breakspear, The connectomics of brain disorders, Nat. Rev. Neurosci. 16 (3) (2015) 159–172.
[15] V. Fleischer, A. Radetz, D. Ciolac, M. Muthuraman, G. Gonzalez-Escamilla, F. Zipp, S. Groppa, Graph theoretical framework of brain networks in multiple sclerosis: a review of concepts, Neuroscience 403 (2019) 35–53.
[16] F.V. Farahani, W. Karwowski, N.R. Lighthall, Application of graph theory for identifying connectivity patterns in human brain networks: a systematic review, Front. Neurosci. 13 (2019) 585.
[17] S. Sadaghiani, M.J. Brookes, S. Baillet, Connectomics of human electrophysiology, NeuroImage 247 (2022) 118788.
[18] M. Yu, O. Sporns, A.J. Saykin, The human connectome in Alzheimer disease—relationship to biomarkers and genetics, Nat. Rev. Neurol. 17 (9) (2021) 545–563.
[19] W.W. Seeley, R.K. Crawford, J. Zhou, B.L. Miller, M.D. Greicius, Neurodegenerative diseases target large-scale human brain networks, Neuron 62 (1) (2009) 42–52.
[20] M.G. Erkkinen, M.-O. Kim, M.D. Geschwind, Clinical neurology and epidemiology of the major neurodegenerative diseases, Cold Spring Harb. Perspect. Biol. 10 (4) (2018) a033118.
[21] H. Shaheen, S. Singh, R. Melnik, A neuron-glial model of exosomal release in the onset and progression of Alzheimer's disease, Front. Comput. Neurosci. 15 (2021) 653097.
[22] H. Shaheen, R. Melnik, Deep brain stimulation with a computational model for the cortex-thalamus-basal-ganglia system and network dynamics of neurological disorders, Comput. Math. Methods 2022 (2022) 8998150, 17.
[23] Y. Zhang, W. Wang, Mathematical analysis for stochastic model of Alzheimer's disease, Commun. Nonlinear Sci. Numer. Simul. 89 (2020) 105347.
[24] S. Fornari, A. Schäfer, E. Kuhl, A. Goriely, Spatially-extended nucleation-aggregation-fragmentation models for the dynamics of prion-like neurodegenerative protein-spreading in the brain and its connectome, J. Theoret. Biol. 486 (2020) 110102.
[25] S. Fornari, A. Schäfer, M. Jucker, A. Goriely, E. Kuhl, Prion-like spreading of Alzheimer's disease within the brain's connectome, J. R. Soc. Interface 16 (159) (2019) 20190356.
[26] E.C. Phillips, C.L. Croft, K. Kurbatskaya, M.J. O'Neill, M.L. Hutton, D.P. Hanger, C.J. Garwood, W. Noble, Astrocytes and neuroinflammation in Alzheimer's disease. 42 (5) (2014) 1321–1325.
[27] R. Thuraisingham, A kinetic scheme to examine the role of glial cells in the pathogenesis of Alzheimer's disease, Metab. Brain Dis. 37 (3) (2022) 801–805.
[28] M.L. Bennett, A.N. Viaene, What are activated and reactive glia and what is their role in neurodegeneration? Neurobiol. Dis. 148 (2021) 105172.
[29] P. Tripathi, N. Rodriguez-Muela, J.R. Klim, A.S. de Boer, S. Agrawal, J. Sandoe, C.S. Lopes, K.S. Ogliari, L.A. Williams, M. Shear, et al., Reactive astrocytes promote ALS-like degeneration and intracellular protein aggregation in human motor neurons by disrupting autophagy through TGF-β1, Stem Cell Rep. 9 (2) (2017) 667–680.
[30] P. Smethurst, H. Franklin, B.E. Clarke, K. Sidle, R. Patani, The role of astrocytes in prion-like mechanisms of neurodegeneration, Brain 145 (1) (2022) 17–26.
[31] S.B. Prusiner, Prions, Proc. Natl. Acad. Sci. 95 (23) (1998) 13363–13383.
[32] M. Jucker, L.C. Walker, Self-propagation of pathogenic protein aggregates in neurodegenerative diseases, Nature 501 (7465) (2013) 45–51.
[33] C. Chavarría, S. Rodríguez-Bottero, C. Quijano, P. Cassina, J.M. Souza, Impact of monomeric, oligomeric and fibrillar alpha-synuclein on astrocyte reactivity and toxicity to neurons, Biochem. J. 475 (19) (2018) 3153–3169.
[34] T.T. Olsson, O. Klementieva, G.K. Gouras, Prion-like seeding and nucleation of intracellular amyloid-β, Neurobiol. Dis. 113 (2018) 1–10.
[35] S.S. Plotkin, N.R. Cashman, Passive immunotherapies targeting aβ and tau in Alzheimer's disease, Neurobiol. Dis. 144 (2020) 105010.
[36] S. Pal, H. Shaheen, R. Melnik, The influence of amyloid-beta on calcium dynamics in Alzheimer's disease: A spatio-temporal study, in: O. Gervasi, B. Murgante, S. Misra, A.M.A.C. Rocha, C. Garau (Eds.), Computational Science and Its Applications- ICCSA 2022, in: Lecture Notes in Computer Science, vol. 13377, Springer, Cham, 2022, pp. 308–322, International Conference on Computational Science and Its Applications.

[37] M.A. Dayeh, G. Livadiotis, S. Elaydi, A discrete mathematical model for the aggregation of β-amyloid, PLoS One 13 (5) (2018) e0196402.
[38] A.J. Dear, G. Meisl, T.C. Michaels, M.R. Zimmermann, S. Linse, T.P. Knowles, The catalytic nature of protein aggregation, J. Chem. Phys. 152 (4) (2020) 045101.
[39] T.B. Thompson, P. Chaggar, E. Kuhl, A. Goriely, Alzheimer's disease neuroimaging initiative, protein-protein interactions in neurodegenerative diseases: A conspiracy theory, PLoS Comput. Biol. 16 (10) (2020) e1008267.
[40] M.M. Pallitto, R.M. Murphy, A mathematical model of the kinetics of β-amyloid fibril growth from the denatured state, Biophys. J. 81 (3) (2001) 1805–1822.
[41] M. Bertsch, B. Franchi, N. Marcello, M.C. Tesi, A. Tosin, Alzheimer's disease: a mathematical model for onset and progression, Math. Med. Biol. A 34 (2) (2017) 193–214.
[42] F. Matthäus, A comparison of modeling approaches for the spread of prion diseases in the brain, in: Modelling Dynamics in Processes and Systems, Springer, 2009, pp. 109–117.
[43] A.N. Kolmogorov, Study of the diffusion equation with growth of the quantity of matter and its application ȶo a problem èbiological soul. 1 (1937) 1–25.
[44] S.B. Prusiner, M. Scott, D. Foster, K.-M. Pan, D. Groth, C. Mirenda, M. Torchia, S.-L. Yang, D. Serban, G.A. Carlson, et al., Transgenetic studies implicate interactions between homologous PrP isoforms in scrapie prion replication, Cell 63 (4) (1990) 673–686.
[45] M.v. Smoluchowski, Drei vortrage uber diffusion, brownsche bewegung und koagulation von kolloidteilchen, Z. Phys. 17 (1916) 557–585.
[46] J.A. Wattis, An introduction to mathematical models of coagulation–fragmentation processes: a discrete deterministic mean-field approach, Physica D 222 (1–2) (2006) 1–20.
[47] J.-F. Collet, Some modelling issues in the theory of fragmentation-coagulation systems, Commun. Math. Sci. 2 (S1) (2004) 35–54.
[48] F. Carbonell, Y. Iturria-Medina, A.C. Evans, Mathematical modeling of protein misfolding mechanisms in neurological diseases: a historical overview, Front. Neurol. 9 (2018) 37.
[49] E.E. Congdon, S. Kim, J. Bonchak, T. Songrug, A. Matzavinos, J. Kuret, Nucleation-dependent tau filament formation: the importance of dimerization and an estimation of elementary rate constants, J. Biol. Chem.s 283 (20) (2008) 13806–13816.
[50] C. Nicholson, K.C. Chen, S. Hrabětová, L. Tao, Diffusion of molecules in brain extracellular space: theory and experiment, Prog. Brain Res. 125 (2000) 129–154.
[51] S.L. Bressler, V. Menon, Large-scale brain networks in cognition: emerging methods and principles, Trends in Cognitive Sciences 14 (6) (2010) 277–290.
[52] R.F. Betzel, D.S. Bassett, Generative models for network neuroscience: prospects and promise, J. R. Soc. Interface 14 (136) (2017) 20170623.
[53] J.A. McNab, B.L. Edlow, T. Witzel, S.Y. Huang, H. Bhat, K. Heberlein, T. Feiweier, K. Liu, B. Keil, J. Cohen-Adad, et al., The Human Connectome Project and beyond: initial applications of 300 mT/m gradients, Neuroimage 80 (2013) 234–245.
[54] B. Szalkai, C. Kerepesi, B. Varga, V. Grolmusz, Parameterizable consensus connectomes from the human connectome project: the budapest reference connectome server v3. 0, Cogn. Neurodyn. 11 (1) (2017) 113–116.
[55] S.I. Cohen, M. Vendruscolo, M.E. Welland, C.M. Dobson, E.M. Terentjev, T.P. Knowles, Nucleated polymerization with secondary pathways.I. Time evolution of the principal moments, J. Chem. Phys. 135 (6) (2011) 08B615.
[56] M. Ries, M. Sastre, Mechanisms of aβ clearance and degradation by glial cells, Front. Aging Neurosci. 8 (2016) 160.
[57] H. Mestre, Y. Mori, M. Nedergaard, The brain's glymphatic system: current controversies, Trends Neurosci. 43 (7) (2020) 458–466.
[58] N.J. Abbott, M.E. Pizzo, J.E. Preston, D. Janigro, R.G. Thorne, The role of brain barriers in fluid movement in the CNS: is there a 'glymphatic'system? Acta Neuropathol. 135 (3) (2018) 387–407.
[59] A.Y. Abramov, M.R. Duchen, The role of an astrocytic NADPH oxidase in the neurotoxicity of amyloid beta peptides, Philos. Trans. R. Soc. B 360 (1464) (2005) 2309–2314.
[60] S. Pal, R. Melnik, Non-Markovian behaviour and the dual role of astrocytes in Alzheimer's disease development and propagation, 2022, arXiv preprint arXiv:2208.03540.
[61] S. Pal, R. Melnik, The role of astrocytes in Alzheimer's disease progression, in: I. Rojas, O. Valenzuela, F. Rojas, L.J. Herrera, F. Ortuño (Eds.), Bioinformatics and Biomedical Engineering, Springer, 2022, pp. 47–58.
[62] Y.S. Kim, H.M. Jung, B.-E. Yoon, Exploring glia to better understand Alzheimer's disease, Anim. Cells Syst. 22 (4) (2018) 213–218.
[63] T.D. Do, N.J. Economou, A. Chamas, S.K. Buratto, J.-E. Shea, M.T. Bowers, Interactions between amyloid-β and tau fragments promote aberrant aggregates: implications for amyloid toxicity, J. Phys. Chem. B 118 (38) (2014) 11220–11230.
[64] A. Serrano-Pozo, M.L. Mielke, T. Gómez-Isla, R.A. Betensky, J.H. Growdon, M.P. Frosch, B.T. Hyman, Reactive glia not only associates with plaques but also parallels tangles in Alzheimer's disease, Am. J. Pathol. 179 (3) (2011) 1373–1384.
[65] C.R. Jack Jr., D.M. Holtzman, Biomarker modeling of Alzheimer's disease, Neuron 80 (6) (2013) 1347–1358.
[66] T.B. Thompson, G. Meisl, T. Knowles, A. Goriely, The role of clearance mechanisms in the kinetics of pathological protein aggregation involved in neurodegenerative diseases, J. Chem. Phys. 154 (12) (2021) 125101.
[67] Y. Wang, M. Martinez-Vicente, U. Krüger, S. Kaushik, E. Wong, E.-M. Mandelkow, A.M. Cuervo, E. Mandelkow, Tau fragmentation, aggregation and clearance: the dual role of lysosomal processing, Hum. Mol. Gen. 18 (21) (2009) 4153–4170.
[68] A.R. Nelson, M.D. Sweeney, A.P. Sagare, B.V. Zlokovic, Neurovascular dysfunction and neurodegeneration in dementia and Alzheimer's disease, Biochim. Biophys. Acta (BBA)-Mol. Basis Dis. 1862 (5) (2016) 887–900.
[69] R.E. Tanzi, L. Bertram, New frontiers in Alzheimer's disease genetics, Neuron 32 (2) (2001) 181–184.
[70] L.D. Goodman, H.J. Bellen, Recent insights into the role of glia and oxidative stress in Alzheimer's disease gained from drosophila, Curr. Opin. Neurobiol. 72 (2022) 32–38.
[71] N. Bhagwat, J.D. Viviano, A.N. Voineskos, M.M. Chakravarty, Alzheimer's Disease Neuroimaging Initiative, et al., Modeling and prediction of clinical symptom trajectories in Alzheimer's disease using longitudinal data, PLoS Comput. Biol. 14 (9) (2018) e1006376.